World Electric Vehicle Journal

MDPI

Article

A Study on Series-Parallel Winding Changeover Circuit and Control Method for Expanding the High-Efficiency Operating Range of IPMSM for xEV Drive Systems

Yangjin Shin [1], Suyeon Cho [2] and Ju Lee [1,*]

[1] Department of Electrical Engineering, Hanyang University, Seoul 04763, Republic of Korea; yjshin@katech.re.kr
[2] Department of Electric Power Train R&D, Korea Automotive Technology Institute, Cheonan 31214, Republic of Korea; sycho@katech.re.kr
* Correspondence: julee@hanyang.ac.kr

Abstract: The motor characteristics control method using the winding changeover technique can improve the matching ratio between the most frequent operating point of electric vehicle (EV) and the motor's high-efficiency operating point, thereby enhancing the overall average efficiency of the drive system. This technology reduces back electromotive force and winding resistance by adjusting the effective number of motor winding turns according to the EV's operating speed, ultimately improving the average efficiency. In this paper, we propose a winding changeover circuit and control method that maximizes the average efficiency in the main driving regions to extend the driving range per charge and improve the fuel efficiency of EVs. The proposed circuit is constructed using thyristor switching devices, offering the advantage of relatively lower overall system losses compared to conventional circuits. Due to the characteristics of the thyristor switching devices used in the proposed circuit, seamless winding changeover is possible during motor operation. Additionally, no extra snubber circuits are required, and the relatively low switch losses suggest the potential for improved efficiency and lightweight design in EV drive systems. To verify the proposed winding changeover circuit and control scheme, experiments were conducted using a dynamometer with an 80 kW permanent magnet motor, inverter, and the developed prototype of the winding changeover circuit.

Keywords: winding changeover circuit; interior permanent magnet synchronous motor (IPMSM); thyristor; electric vehicle (EV)

Citation: Shin, Y.; Cho, S.; Lee, J. A Study on Series-Parallel Winding Changeover Circuit and Control Method for Expanding the High-Efficiency Operating Range of IPMSM for xEV Drive Systems. *World Electr. Veh. J.* **2024**, *15*, 501. https://doi.org/10.3390/wevj15110501

Academic Editor: Grzegorz Sierpiński

Received: 30 September 2024
Revised: 24 October 2024
Accepted: 25 October 2024
Published: 31 October 2024

1. Introduction

The global automotive market is expected to rapidly shift towards high-efficiency internal combustion engines, alternative fuels, and low-emission vehicles due to increasing fuel cost burdens from oil price fluctuations and tightening CO_2 emission regulations. Furthermore, major organizations such as the DOE project that eco-friendly vehicles will account for more than 50% of the market within the next decade [1,2]. As a result, with the expansion of the eco-friendly vehicle market, competition is intensifying, focusing on technologies that improve the fuel efficiency of EVs [3–6].

The interior permanent magnet synchronous motor (IPMSM), primarily used as the drive system for EVs, offers higher efficiency compared to engines, reduces vibration and noise issues, and enables precise and accurate torque control across the entire speed range [7]. Therefore, unlike conventional engine vehicles, most electric drive systems are equipped with a reduction gear with a fixed reduction ratio, allowing the vehicle to be driven over the entire speed range without a separate mechanical transmission system.

Figure 1 shows the efficiency map for the entire driving range of the IPMSM, overlapping the main driving points according to the two driving modes of the vehicle. As can be seen in the figure, the frequently utilized operating areas of the vehicle are characterized by

a division between low-speed, high-torque conditions in urban settings and high-speed, low-torque conditions on highways. In contrast, the high-efficiency region of the optimally designed IPMSM is distributed in the area marked in blue. Therefore, as shown in Figure 1, there is a mismatch between the most frequently used operating points of the EV and the high-efficiency region of the IPMSM. Since the full charge range of the EV is determined by the average efficiency range, not the highest efficiency point of the electric motor, the expected driving distance of the EV is bound to be shorter than the motor performance.

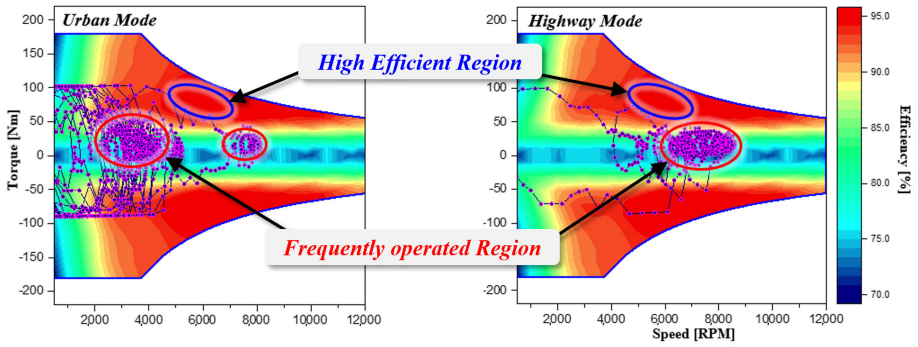

Figure 1. Efficiency map of the IPMSM for the entire driving range with overlapping main driving points of the two driving modes.

Since increasing the peak efficiency of the motor is becoming increasingly difficult from a design perspective and is already reaching saturation, it is more important for EV motors to expand the range of average high efficiency. Alternatively, even if the motor's peak efficiency is not high, expanding the range of high efficiency can enhance the actual driving efficiency of the vehicle. Therefore, in order to solve this problem, there is an increasing demand for the development of a changeover system that changes the characteristics of the motor according to the driving speed of the EV so that the efficiency of the main operating points can be improved [8].

Figure 2 illustrates the torque-speed curves for each operating mode of the two-speed changeover system. By adjusting the motor characteristics to match the operating range of the EV, high-efficiency operation can be achieved over a wide speed range.

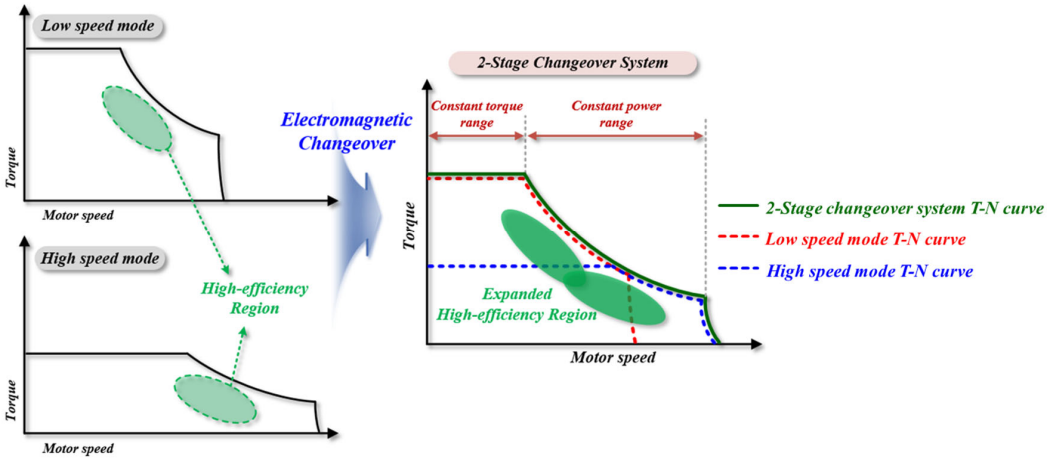

Figure 2. Torque-Speed characteristics of two-stage changeover system.

The methods for altering the motor characteristics can be broadly divided into two categories: varying the flux linkage or adjusting the winding configuration. The method of varying magnetic flux can lead to increased mechanical complexity, resulting in a larger overall drive system size, and may complicate the switching process during vehicle operation, making it unsuitable for application in EVs. Therefore, this paper selects the

winding changeover method, which is relatively simple in terms of mechanical structure and easy to control, allowing for changeover during operation and making it more suitable for vehicle applications.

The method of adjusting the motor's windings involves changing the winding connections or altering the effective turn count to regulate the back electromotive force, thereby expanding the inverter's motor control range [9,10]. In EV drive systems, circuits that change the winding structure of the motor are actively being developed, primarily in Japan, and are also being applied to home appliances such as washing machines and wind power systems [11,12]. However, the winding changeover systems composed of conventional mechanical switches have a limited circuit lifespan. Moreover, since the method requires stopping the motor to change the connections via switches before restarting, it results in long changeover times and interruptions in motor current and torque, posing limitations for application in EVs. To address the issues associated with mechanical switches, changeover circuits using electrical switches have been developed, including Δ-Y configurations, neutral-point changeover systems, and other variable-phase configurations [13–17]. The variable-phase configuration can achieve relatively high-efficiency in the changeover circuit, but it has the disadvantage of increased complexity in the changeover circuit components [18]. The Δ-Y winding changeover circuit reduces interruptions in motor current and torque due to shorter changeover times; however, its low changeover ratio makes it difficult to achieve the average high efficiency required for EVs [19]. In the case of neutral-point changeover circuits, while the control is straightforward, the need for additional snubber circuits during the changeover and the significant losses incurred in the circuit are notable disadvantages. Although existing changeover circuits have proposed various circuit structures, they lack sufficient analysis of the efficiency characteristics related to the additional power consumption incurred by each model. This paper aims to analyze the power consumption of the components used when optimizing the design of the changeover circuit based on the specified motor characteristics, while also establishing specific applicability regarding vehicles in terms of component costs.

Meanwhile, a leading Japanese company has implemented its proprietary electromagnetic changeover system in EVs, significantly expanding the high-efficiency operating range within the main driving region [20–22]. This circuit utilizes a minimal number of IGBT switches and diodes, effectively addressing the limited lifespan issues of traditional mechanical switches while also reducing changeover time. However, to dissipate the residual energy from the motor winding inductors during the changeover, a separate snubber circuit composed of R-C-D is required. Additionally, high conduction losses occurring in the IGBT switches of the changeover circuit can reduce the power density of the drive system.

This paper proposes a changeover circuit utilizing thyristor switch and conducts a comparative analysis with existing advanced changeover circuits. The proposed changeover circuit employs thyristors to connect the motor windings in series during low-speed operation and in parallel during high-speed operation, thereby enabling the achievement of high efficiency for EVs across a wide operating range [23]. Furthermore, the use of thyristors during the changeover enables seamless operation without interruption, eliminating the need for a separate snubber circuit. Additionally, the relatively low losses in the drive system can enhance the fuel efficiency and reduce the weight of EVs. To verify the vehicle applicability of the proposed changeover circuit, performance was demonstrated through dynamometer testing in conjunction with an inverter and an 80 kW IPMSM featuring an altered winding structure.

2. Conventional Changeover Circuit

This paper introduces the changeover circuit commercialized by leading companies and the proposed circuit, providing a comparative analysis of their losses and costs. Figure 3 illustrates the neutral-point shift type two-speed changeover circuit that has been commercialized.

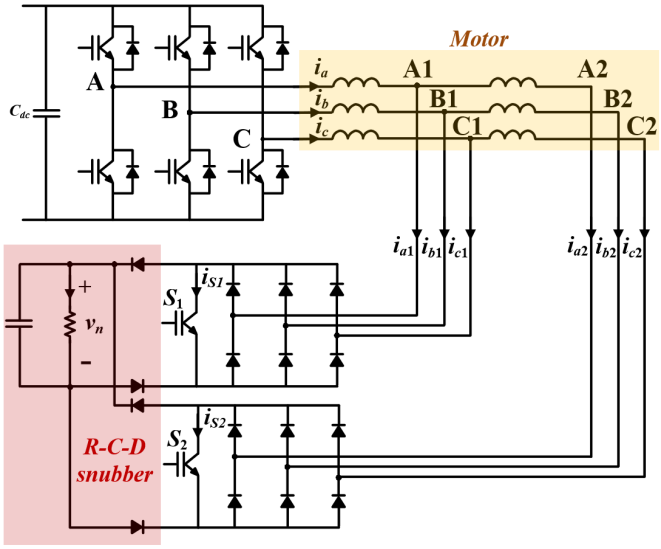

Figure 3. The structure of the conventional changeover circuit.

This two-speed changeover circuit consists of an IGBT switch, a three-phase diode rectifier, and an R-C-D snubber. During low-speed operation, S1 is turned off and S2 is turned on, short-circuiting A2, B2, and C2 of the motor in a Y-connection, allowing the use of the entire motor winding. During high-speed operation, S1 is turned on, short-circuiting A1, B1, and C1 in a Y-connection, which enables the use of only half of the motor winding. In the figures, i_a, i_b, and i_c represent the output currents of the inverter. i_{a1}, i_{b1} and i_{c1} indicate the phase currents when only half of the motor windings are used during high-speed operation. Conversely, during low-speed operation when all motor windings are used, i_{a2}, i_{b2} and i_{c2} represent the phase currents of the motor.

The winding connections and back electromotive force of the motor during high-speed and low-speed operation in this circuit can be represented using vector diagrams, as shown in Figure 4. In the first low-speed mode, where the back electromotive force is small, all windings are used, while in the second high-speed mode, the use of motor windings is reduced to lower the back electromotive force, thereby expanding the motor's operating range.

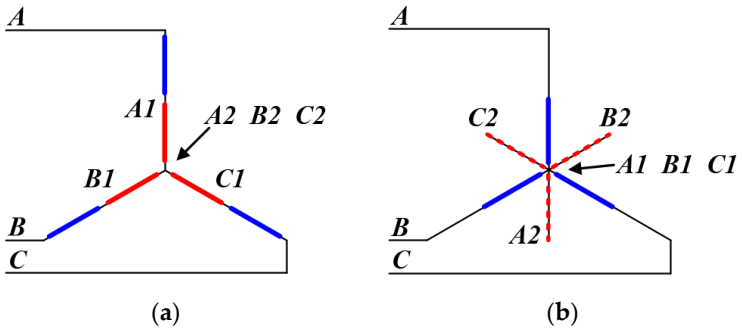

Figure 4. Voltage vector diagrams according the winding connections in the conventional neutral-point shift type changeover circuit. (**a**) Low-speed mode; (**b**) high-speed mode.

This circuit addresses the limited lifespan issues of conventional mechanical switch-based changeover circuits. Additionally, it allows for switching operations during driving using electrical switches, thus reducing the winding changeover time. Additionally, this changeover circuit is highly stable from a circuit perspective and offers the advantages of a very simple design and control method. Figure 5 shows the simulation waveforms during the winding changeover operation of this circuit. i_a, i_b, and i_c represent the output phase currents of the inverter, while i_{a1}, i_{b1} and i_{c1} represent the phase currents when only half of

the windings are used in high-speed mode. i_{S1} and i_{S2} indicate the currents flowing through the IGBTs in high-speed and low-speed modes, respectively. The simulation waveforms show the operation where the motor windings are fully utilized in low-speed mode (with $S1$ off and $S2$ on), then changeover to high-speed mode when $S1$ turns on.

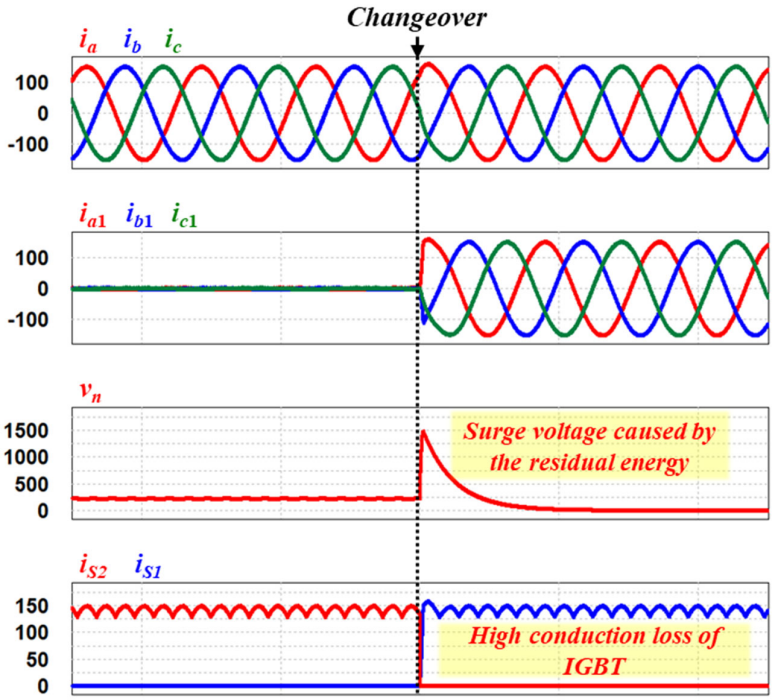

Figure 5. Simulation results of the conventional changeover circuit.

During steady-state operation, significant conduction losses occur in the IGBT and diode rectifier of the changeover circuit, as shown in Figure 5. In particular, since the three-phase AC current rectified into DC flows entirely through the IGBT switch, approximately half of the total losses in the changeover circuit occur in the IGBT. Therefore, a drawback is that the cooling system size may need to increase due to the heat generated by the circuit losses. Additionally, a separate passive snubber circuit, consisting of R-C-D components, is required to dissipate the residual energy in the motor that may be generated during winding changeover. Since the winding changeover event occurs only occasionally, the energy dissipated in the snubber circuit can be considered negligible. Additionally, the neutral-point shift type changeover circuit has the characteristic of a lower utilization rate of the motor windings in high-speed mode, as only half of the windings are used. On the other hand, in this paper, the research was conducted with the original goal of improving the actual driving efficiency of vehicles, focusing on a winding changeover method that not only performs its function but also reduces the associated losses compared to conventional circuits.

3. Proposed Changeover Circuit

The proposed changeover circuit, as shown in Figure 6, is composed of thyristor switching devices and employs a method that switches the windings between series and parallel configurations. The proposed circuit consists of switches (S_{0p}, S_{0n}) that connect the motor windings in series, and switches (S_{1p}, S_{1n}, S_{2p}, S_{2n}) that connect the windings in parallel, for each phase. This circuit allows the motor windings to be switched from series to parallel and from parallel to series.

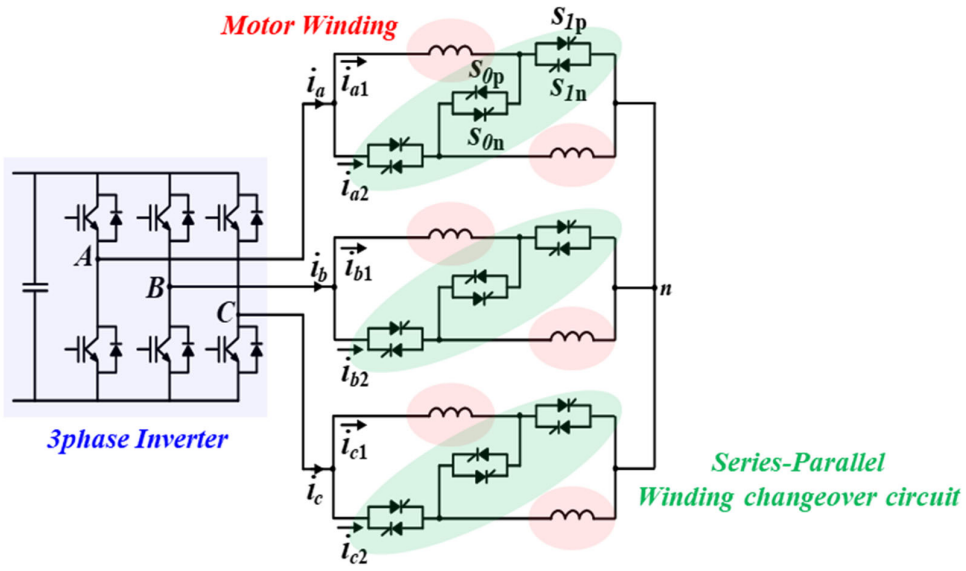

Figure 6. Proposed series-parallel winding changeover circuit.

Figure 7 shows the connection status of the proposed circuit according to the motor speed. At low speeds, the circuit is configured in series to utilize the cumulative BEMF, while at high speeds, due to voltage limitation issues, the circuit is configured in parallel to reduce the BEMF. By altering the Torque-Speed characteristics of the IPMSM according to each speed mode, high efficiency can be achieved across a wide speed range. Additionally, the proposed changeover circuit utilizes the characteristics of thyristor switching devices, allowing for the switching of motor windings between series and parallel configurations without the need for a separate snubber circuit.

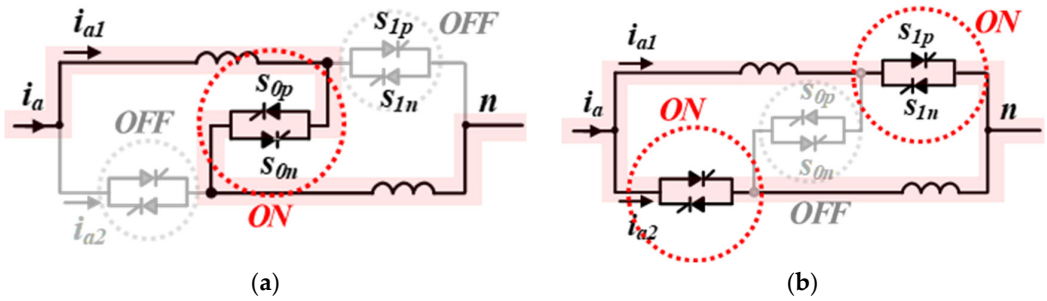

Figure 7. Connection status of the proposed changeover circuit based on motor speed. (**a**) Low-speed mode; (**b**) high-speed mode.

Figure 8 illustrates the thyristor switching operation in the proposed changeover circuit. By alternating the S_P switch during the positive cycle and the S_N switch during the negative cycle, in accordance with the current phase, the motor current flows continuously without interruption. Rather than switching at the zero-crossing point where the positive and negative cycles of the current change, a gate signal is applied to the switch in advance to ensure safe current conduction. Since the gate signal of the thyristor switching device is driven by current, there may be a delay in the switching timing. To prevent circuit malfunction due to this delay, the gate signal must be turned on in advance, before the zero-crossing point is reached. Since the thyristor switching device only turns on when forward current flows, even if the gate signal is applied, it is safer circuit-wise to apply the gate signal in advance. Similarly, the turn-off condition of the thyristor ensures that, even if the gate signal is applied, the switch will stop conducting once reverse current flows, allowing the switch to be turned off safely. However, due to current ripple or harmonic distortion occurring at the zero-current point, a small amount of forward current may

still flow briefly after the zero-crossing point. Therefore, it is important not to turn off the thyristor switch signal immediately at the zero-crossing point, but to allow sufficient time after the point before turning off the gate signal. As a result, there will be an overlap period between the gate signals of the upper and lower thyristor switches. This overlap ensures safe conduction, even for distorted current waveforms that contain harmonics. To control the bidirectional switch using thyristors as described above, the phase information of the conduction current for each phase is essential. However, the phase information provided by the inverter corresponds to the rotor position used in the current vector control algorithm. If the inverter's current controller is sufficiently tuned, the phase command information of the current vector can be used to determine the zero-crossing phase angle of the current for each phase as shown in Figure 9.

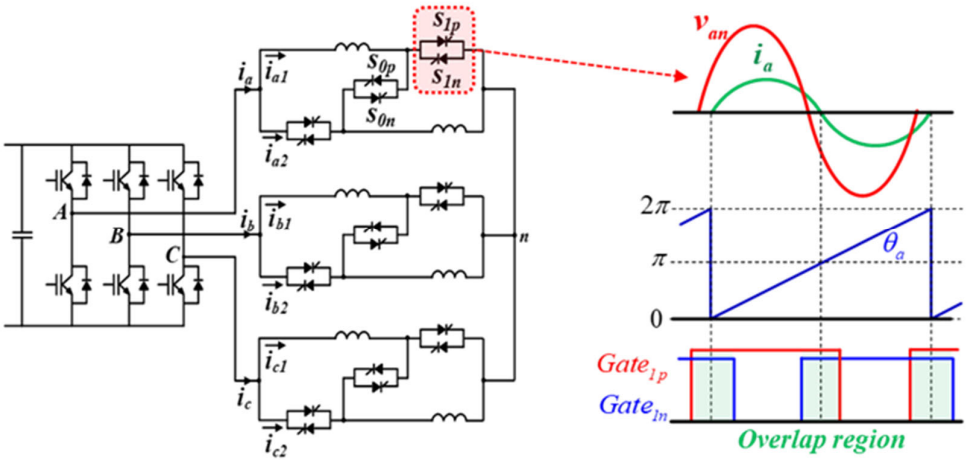

Figure 8. Thyristor switching operation in the proposed changeover circuit.

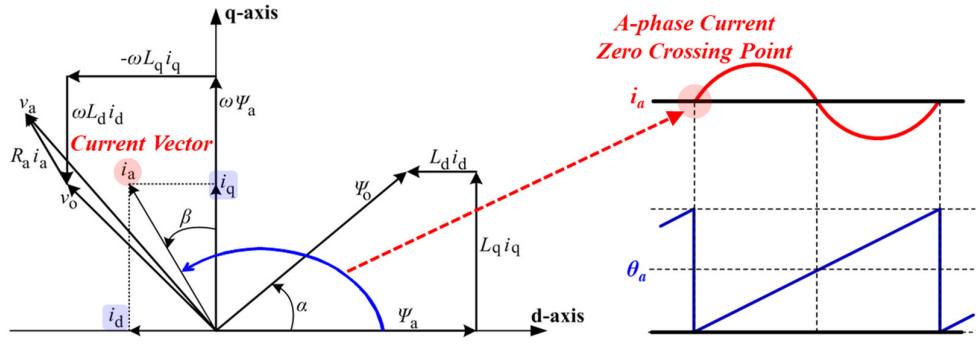

Figure 9. Phase angle detection for current zero-crossing in the proposed changeover circuit.

Figure 10 illustrates the control method for the thyristor gate signals when a switching signal is input during operation. When a changeover signal is input, the circuit wiring is not changed immediately, but the changeover operation is performed at the next zero-crossing point. The current is allowed to flow while maintaining the existing motor winding connections. As the next zero-crossing point approaches, the gate signal for the current connection is discontinued, and the gate signal for the desired connection is applied, thereby executing the changeover operation. Thyristors automatically turn off when the conducting current falls below the holding current; thus, if the next gate signal is not applied, current will cease to flow through the original connection at zero current. Consequently, current will continuously flow through the altered connection. There is a slight delay in the changeover signal, however, the uninterrupted winding changeover operation can be performed during driving, eliminating the need for an additional snubber circuit.

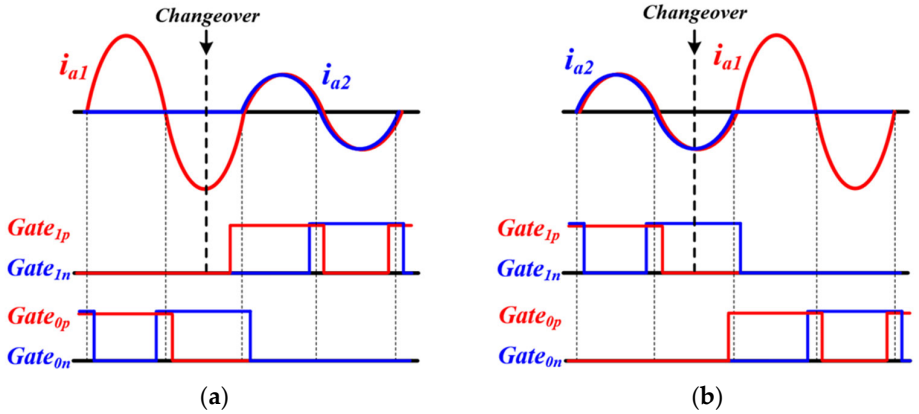

Figure 10. Control method for thyristor gate signals during changeover operation. (**a**) Series, low-speed mode to parallel, high-speed mode; (**b**) parallel, high-speed mode to series, low-speed mode.

Figure 11 illustrates the simulation waveforms during the changeover operation according to the speed mode, applying the switching method of the changeover circuit presented earlier. Before the changeover signal is input, it can be observed that the thyristor gate signals are applied in accordance with the phase of the conducting current. When the changeover signal is received, the switch that was conducting current turns off at the next zero-crossing point, and the switch that configures the desired connection begins to turn on, thereby performing the changeover operation. Unlike conventional changeover circuits, it can be confirmed that there is no overcurrent or overvoltage generated during the switching process, allowing for safe changeover.

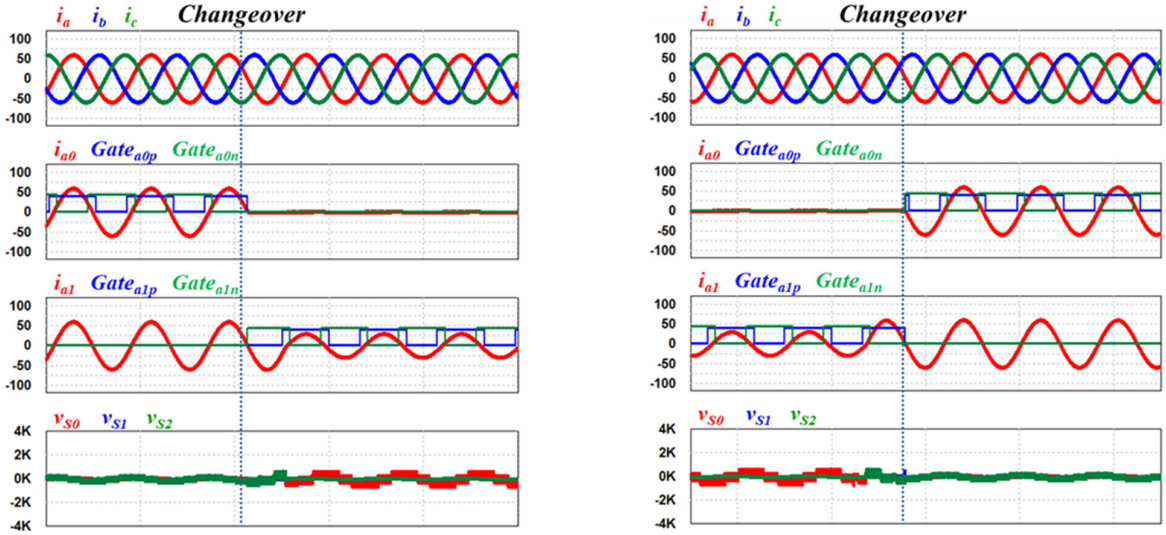

Figure 11. Simulation waveforms during changeover operation. (**a**) Series, low-speed mode to parallel, high-speed mode; (**b**) parallel, high-speed mode to series, low-speed mode.

Figure 12 illustrates the simulation waveforms of the switching operation when the ripple component of the motor current is large and when low-order harmonic components are significantly present. As shown in the waveforms, in cases of severe current distortion, the current direction changes rapidly between positive and negative near the zero-crossing point. By setting the bidirectional thyristor gate signals to overlap at the zero-crossing point, as proposed in the switching method, even distorted currents, as shown in the waveform, can flow continuously without interruption.

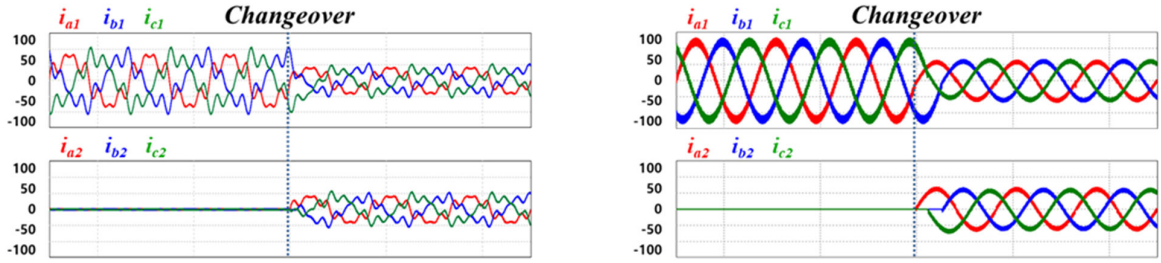

(**a**) (**b**)

Figure 12. Simulation waveforms during changeover operation for distorted currents. (**a**) Series, low-speed mode to parallel, high-speed mode; (**b**) parallel, high-speed mode to series, low-speed mode.

4. Comparative Analysis

In this chapter, a comparative analysis of the losses and costs associated with the existing changeover circuit and the proposed changeover circuit designed for an 80 kW motor specification will be conducted. First, to evaluate the applicability to the driving system of EVs, suitable switching devices that meet the design specifications will be selected. For comparative analysis, the selected IGBT in the existing changeover circuit is Infineon's FZ800R12KE3, and the three-phase diode rectifier is IXYS's VUO190-08NO7. In the proposed changeover circuit, the selected thyristor is IXYS's MCC310-16io1.

Figure 13 shows the current specifications of the main components in the existing changeover circuit according to the speed mode. Based on the shown current specifications and the data for each selected component, the conduction loss is calculated at 123 W per diode, totaling 739 W for the three-phase diode rectifier. For the IGBT, the loss is calculated at 1108 W, resulting in a total circuit loss of 1847 W. This accounts for approximately 2.31% of the entire drive system for the 80 kW specification. While losses occur in the three-phase diode rectifier, it is evident that the standalone losses generated by the IGBT are significantly larger. These losses can be comparable to the losses generated in the drive inverter, necessitating a significantly large cooling system to manage the heat generated by such losses.

Figure 14 shows the current specifications of the thyristor component in the proposed circuit according to the speed mode. Based on the shown current specifications and the data for the selected thyristor, the conduction loss is calculated at 216 W per switch in series, resulting in a total circuit loss of 1296 W. Although the current is halved in parallel connection, the number of conducting switches doubles, keeping the total loss value the same. This accounts for approximately 1.62% of the entire drive system.

Figure 15 presents a graphical comparison of the losses and costs incurred by the two circuits. The total loss of the proposed circuit is approximately 30% lower compared to the existing circuit, allowing for a reduction in the volume of the cooling system. Moreover, in the existing circuit, high losses occur in specific components, leading to significant thermal imbalance. As a result, the design of the cooling system may be more complex compared to the proposed circuit, where heat is more evenly distributed. However, the proposed circuit has a higher number of switches compared to the existing circuit, requiring more driving circuit components. Therefore, it is evident that the total cost is higher. Although the proposed circuit requires a larger number of components and has a relatively complex control method, it offers the advantage of minimizing losses, allowing for a more compact heat dissipation system and improving overall drive efficiency.

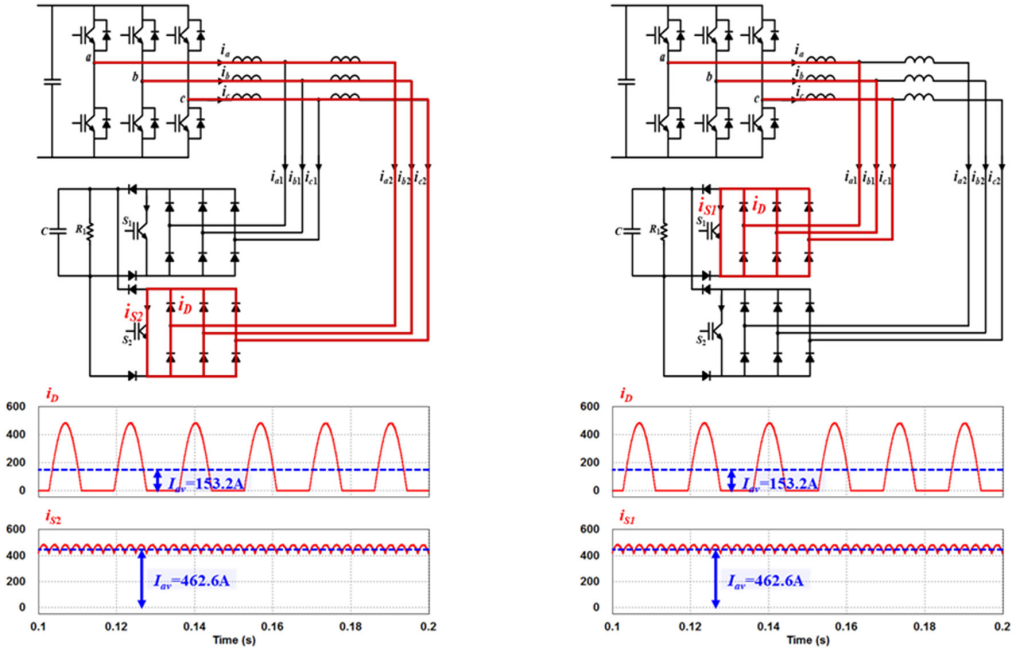

(**a**) (**b**)

Figure 13. Current specification of main components in the conventional changeover circuit by speed mode at 80 kW. (**a**) Low-speed mode; (**b**) high-speed mode.

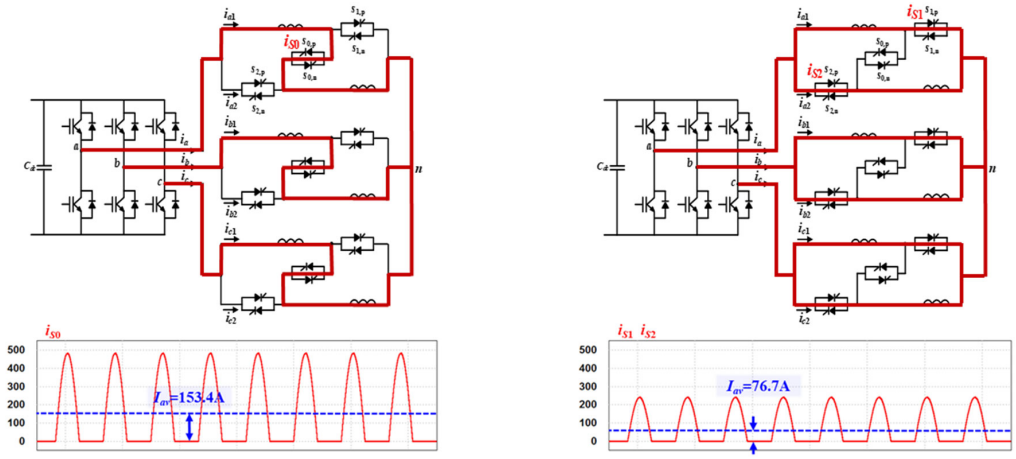

(**a**) (**b**)

Figure 14. Current specification of thyristor in the proposed changeover circuit by speed mode at 80 kW. (**a**) Series, low-speed mode; (**b**) parallel, high-speed mode.

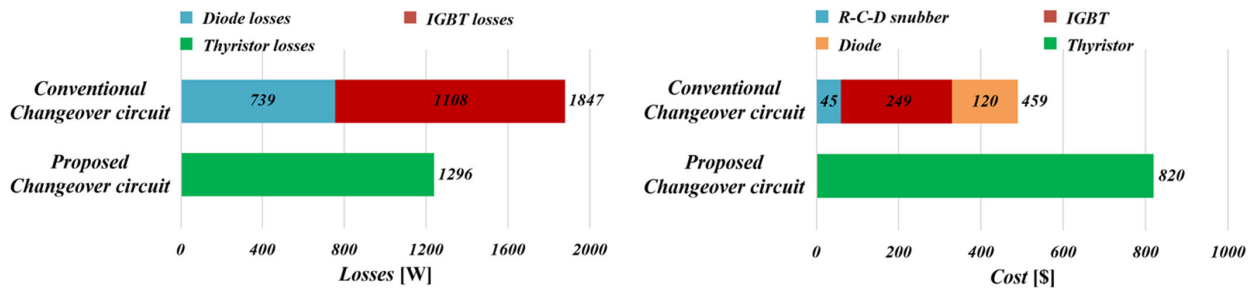

(**a**) (**b**)

Figure 15. Comparison of losses and costs between the proposed and conventional changeover circuit. (**a**) Loss comparison at 80 kW; (**b**) costs comparison.

5. Experimental Results

To verify the feasibility of the proposed changeover circuit, a dynamometer test was performed using an 80 kW IPMSM along with an inverter, as illustrated in Figure 16. Tables 1 and 2 show the motor output specifications of the developed motor based on the winding configuration. Figure 17 shows the experimental waveforms obtained from the dynamometer test of a prototype of the proposed changeover circuit rated at 80 kW. The waveforms were measured while operating in the low-speed mode with series connection and in the high-speed mode with parallel connection. i_a represents the phase A current output from the inverter, while i_{a1} and i_{a2} refer to the currents flowing through the upper and lower windings, respectively, as shown in the winding configuration. In the series connection, the same current flows through all windings, but in the parallel connection, the current splits equally, with i_{a1} and i_{a2} each carrying half of i_a.

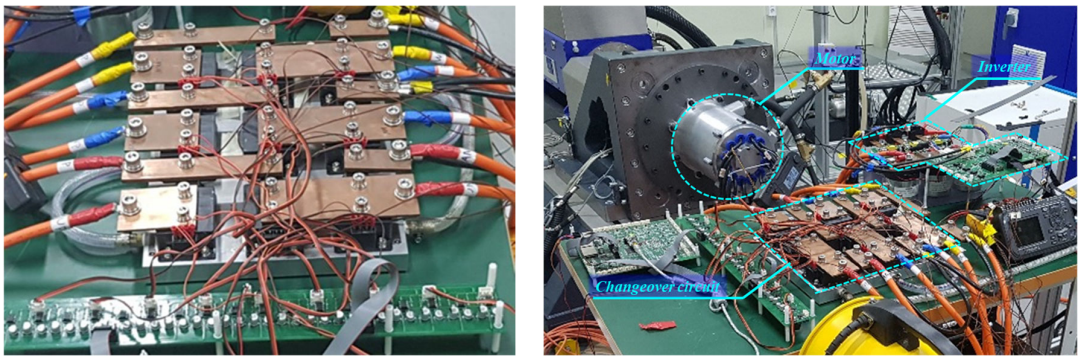

(**a**) (**b**)

Figure 16. Dynamometer test setup for the proposed 80 kW changeover circuit with IPMSM and inverter. (**a**) Prototype of the proposed changeover circuit; (**b**) experimental setup.

Table 1. Motor output specification for series winding configuration.

Parameters	Base Speed	Maximum Speed
Speed	3000 RPM	6000 RPM
Torque	318.4 Nm	159.3 Nm
Line-to-Line Voltage	188.5 Vrms	212.5 Vrms
Phase Voltage	109.8 Vrms	126.4 Vrms
Phase Current	361.5 Arms	337.5 Arms

Table 2. Motor output specification for parallel winding configuration.

Parameters	Base Speed	Maximum Speed
Speed	6000 RPM	10,000 RPM
Torque	159.4 Nm	95.7 Nm
Line-to-Line Voltage	169.5 Vrms	212.4 Vrms
Phase Voltage	98.4 Vrms	123.4 Vrms
Phase Current	365.5 Arms	305.0 Arms

Figure 18 shows the current waveforms in each winding during the winding changeover operation under driving conditions. Additionally, it also presents the gate waveform of the series switch, confirming that the thyristor gate signal alternates properly at the zero-crossing point in accordance with the proposed switching method, ensuring uninterrupted current conduction. However, since the winding changeover alters not only the motor parameters but also the back electromotive force (back EMF) and the applied current command map, it may appear to the drive inverter as though the motor has suddenly changed. Therefore, the transient current at the moment of winding changeover can become significantly large. Additionally, due to the nature of the proposed control method, where

the switching sequence of each phase current differs based on the individual phases in the three-phase system, the transient current during the changeover can become even larger. To address this, we ensure that the feedforward control components for the current commands are always updated according to the motor model to prepare for the changeover operation. Since the high-speed region is characterized by a large BEMF the applied voltage changes significantly during winding changeover, leading to large transient currents. Similarly, in regions with high torque load, winding changeover affects the fluctuation of output torque, which negatively impacts noise, vibration, and overall drivability. To minimize transient currents during the changeover process, we conducted experiments by limiting the changeover regions to relatively low-speed and low-torque areas.

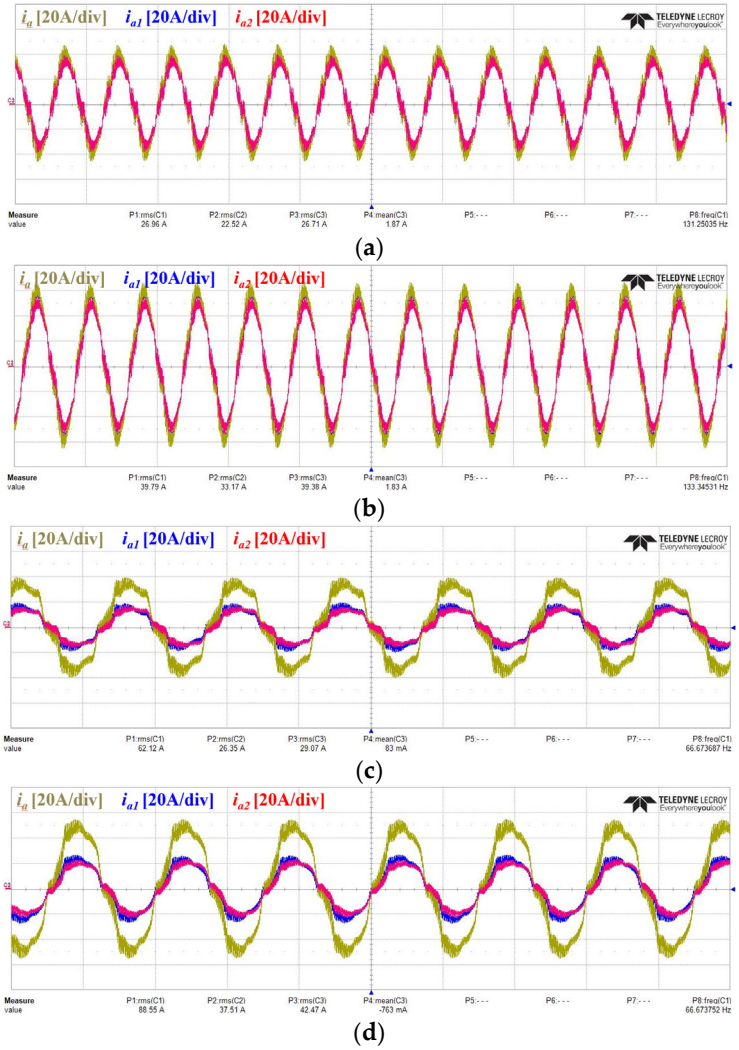

Figure 17. Experimental waveforms from the dynamometer test of the 80 kW changeover circuit. (**a**) Series, low-speed mode at 2000 RPM, 20 Nm; (**b**) series, low-speed mode at 2000 RPM, 30 Nm; (**c**) parallel, high-speed mode at 1000 RPM, 20 Nm; (**d**) parallel, high-speed mode at 1000 RPM, 30 Nm.

Figure 19 shows the experimental waveforms of the winding changeover with and without the addition of feedforward components in the drive inverter's current controller. The transient current generated at the changeover point ultimately affects the motor's output torque. Therefore, to minimize fluctuations in output torque at the changeover point, it is essential to minimize the transient current. As shown in the figure, the feedforward component compensated in the inverter controller at the changeover point is crucial for reducing the transient current.

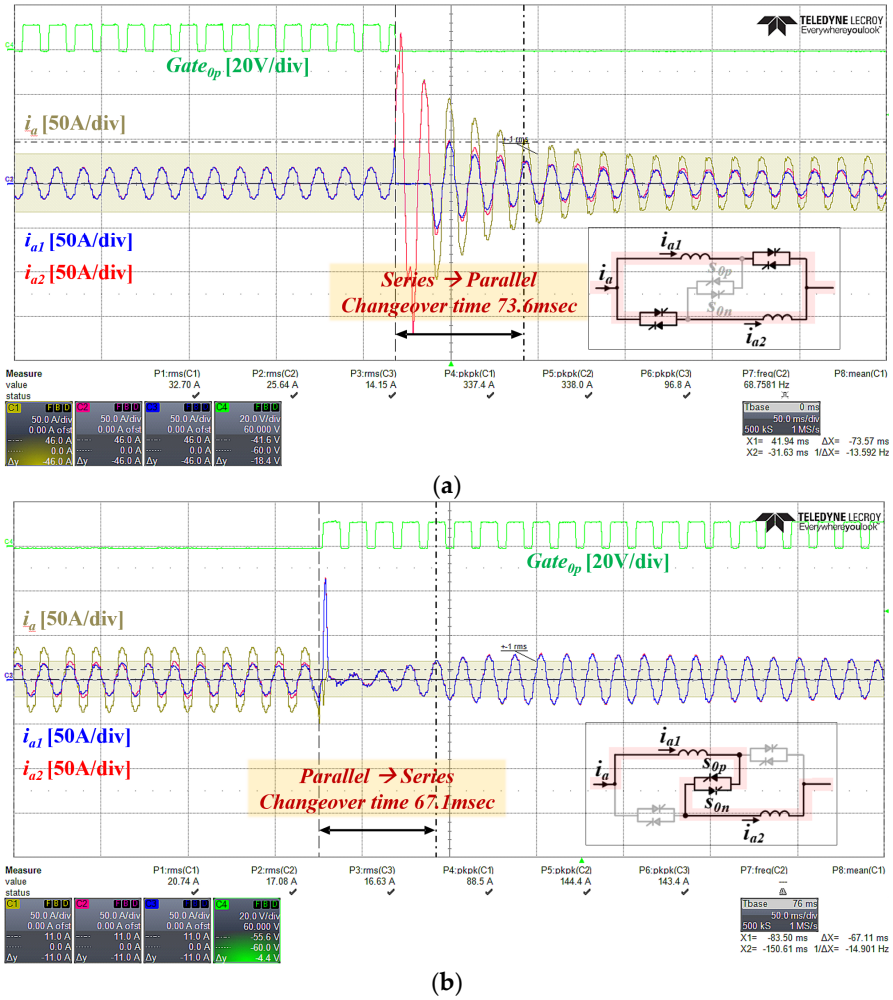

Figure 18. Current and gate waveforms during winding changeover operation in the proposed circuit at 1000 RPM, 10 Nm. (**a**) Series, low-speed mode to parallel, high-speed mode; (**b**) parallel, high-speed mode to series, low-speed mode.

The time required to change over from low-speed, series mode to high-speed, parallel mode was approximately 73.57 ms. Conversely, the time required to change over from high-speed, parallel mode to low-speed, series mode was approximately 67.11 ms as shown in Figure 18. The winding changeover time was measured as the time taken for the current to reach within 80% of the commanded value.

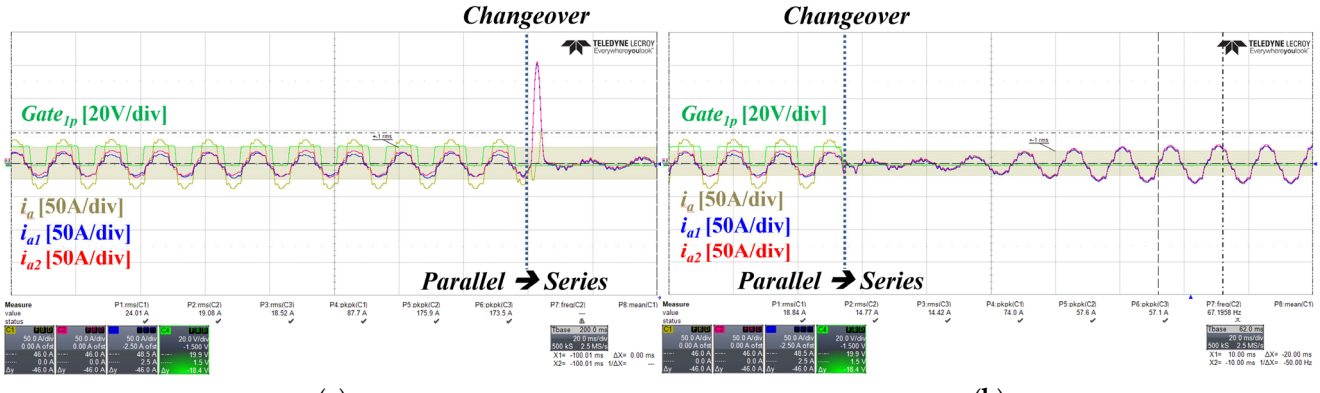

Figure 19. *Cont.*

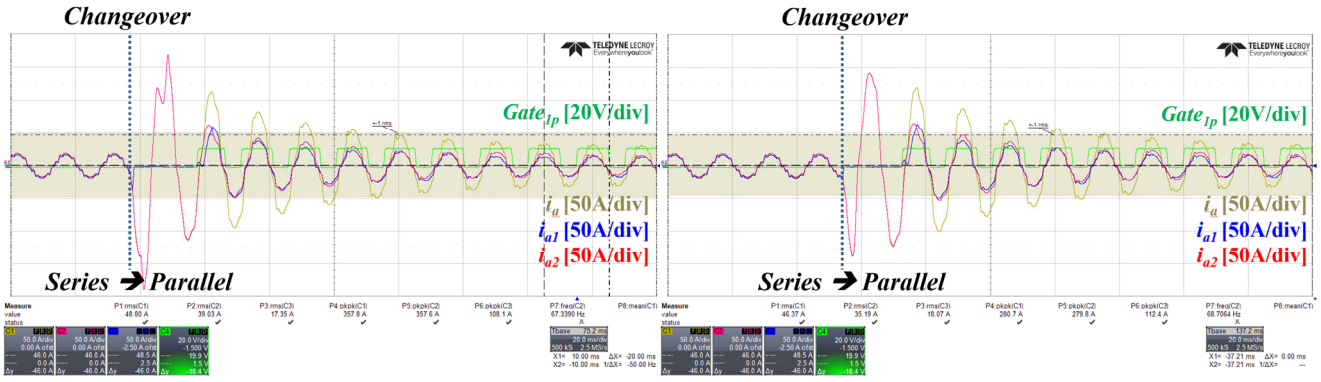

(**c**) (**d**)

Figure 19. Current and gate waveforms during winding changeover operation with and without inverter controller feedforward at 1000 RPM, 10 Nm. (**a**) Parallel, high-speed mode to series, low-speed mode without feedforward; (**b**) parallel, high-speed mode to series, low-speed mode with feedforward; (**c**) series, low-speed mode to parallel, high-speed mode without feedforward; (**d**) series, low-speed mode to parallel, high-speed mode with feedforward.

Figure 20 illustrates the efficiency maps of the motor, inverter, and the overall drive system based on the winding configuration. Observing the integrated motor efficiency map across the entire speed range, it can be seen that the high-efficiency region has expanded. Consequently, the high-efficiency region of the overall drive system has also expanded.

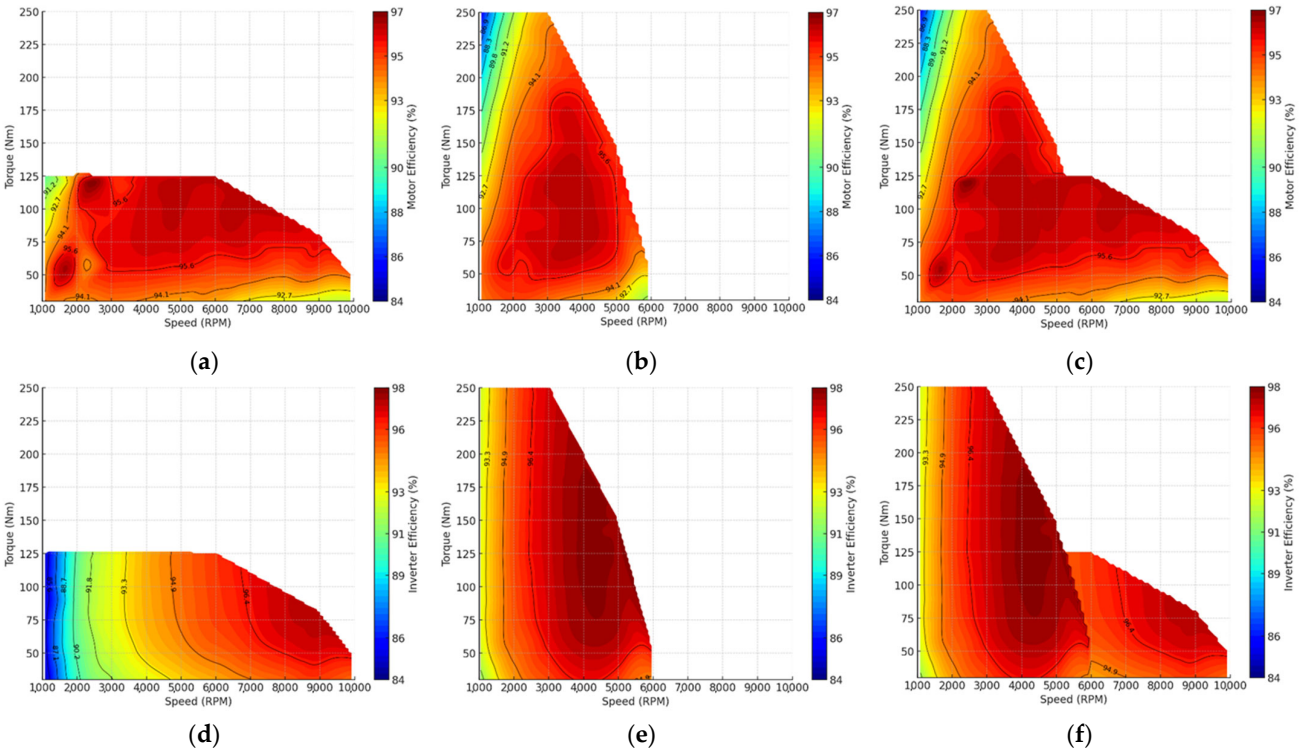

(**a**) (**b**) (**c**)

(**d**) (**e**) (**f**)

Figure 20. *Cont.*

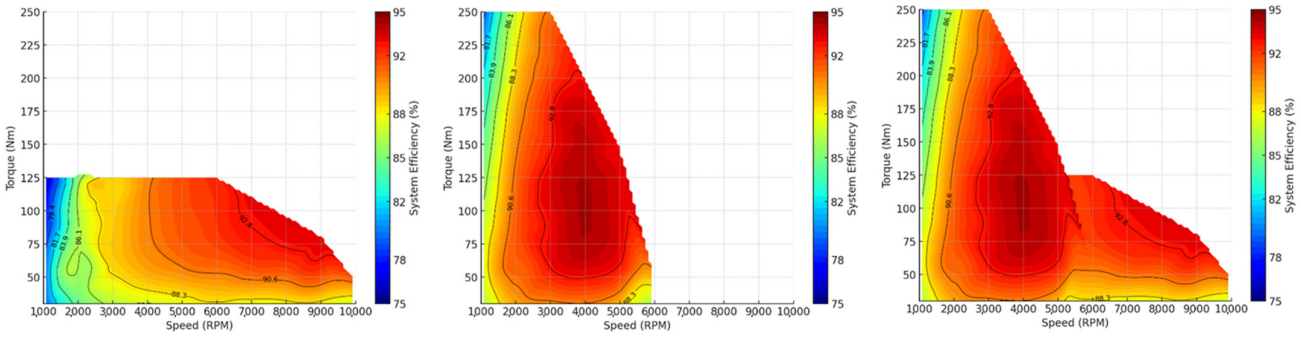

Figure 20. Efficiency map based on winding configuration. (**a**) Motor efficiency map for parallel winding; (**b**) motor efficiency map for series winding; (**c**) integrated motor efficiency map for the entire speed range; (**d**) inverter efficiency map for parallel winding; (**e**) inverter efficiency map for series winding; (**f**) integrated inverter efficiency map for the entire speed range; (**g**) system efficiency map for parallel winding; (**h**) system efficiency map for series winding; (**i**) integrated system efficiency map for the entire speed range.

6. Conclusions

This paper proposes a changeover circuit that utilizes winding switching technology to adjust the electromagnetic characteristics of the motor, enabling the operating range of the EV to coincide with the motor's high-efficiency zone. The proposed changeover circuit switches the motor's connections between series and parallel during operation, thereby altering the motor characteristics according to the speed range. Compared to the mechanical switches used in the previous changeover circuit, the circuit resolves lifespan issues and enables rapid winding changeover. Additionally, by utilizing thyristors, it was possible to minimize the transients that occur during the changeover. While the proposed circuit has a higher number of components and may be priced higher compared to the existing circuit, it offers the advantage of lower conduction losses, allowing for expectations of improved efficiency and lightweight design in the changeover system. A prototype of the proposed circuit rated at 80 kW was developed, and its changeover operation was verified through experiments by integrating it with an IPMSM and inverter. While winding changeover technology has not yet reached mass production, it has secured a foundation for quicker accessibility when the need arises in the future.

Author Contributions: Conceptualization, Y.S., S.C. and J.L.; methodology, Y.S. and S.C.; software, Y.S.; validation, Y.S. and S.C.; formal analysis, Y.S.; investigation, S.C.; data curation, Y.S.; writing—original draft preparation, Y.S.; writing—review and editing, J.L.; supervision, J.L.; project administration, J.L. All authors have read and agreed to the published version of the manuscript.

Funding: This research was supported by the Automotive Industry Technology Development Program (2410000502, Development of High-Efficiency and High-Density Electric Vehicle Inverter based on GaN Power Module) funded by the Ministry of Trade, Industry & Energy(MOTIE, Korea).

Data Availability Statement: The original contributions presented in this study are included in the article. Further inquiries can be directed to the corresponding author.

Conflicts of Interest: The authors declare no conflicts of interest.

References

1. Husain, I.; Ozpineci, B.; Islam, S.; Gurpinar, E.; Su, G.-J.; Yu, W.; Chowdhury, S.; Xue, L.; Rahman, D.; Sahu, R. Electric Drive Technology Trends, Challenges, and Opportunities for Future Electric Vehicles. *Proc. IEEE* **2021**, *109*, 1039–1059. [CrossRef]
2. Aghabali, I.; Bauman, J.; Kollmeyer, P.J.; Wang, Y.; Bilgin, B.; Emadi, A. 800-V Electric Vehicle Powertrains: Review and Analysis of Benefits, Challenges, and Future Trends. *IEEE Trans. Transp. Electrif.* **2021**, *7*, 927–948. [CrossRef]
3. Reimers, J.; Dorn-Gomba, L.; Mak, C.; Emadi, A. Automotive Traction Inverters: Current Status and Future Trends. *IEEE Trans. Veh. Technol.* **2019**, *68*, 3337–3350. [CrossRef]

4. Puma-Benavides, D.S.; Calderon-Najera, J.d.D.; Izquierdo-Reyes, J.; Galluzzi, R.; Llanes-Cedeño, E.A. Methodology to Improve an Extended-Range Electric Vehicle Module and Control Integration Based on Equivalent Consumption Minimization Strategy. *World Electr. Veh. J.* **2024**, *15*, 439. [CrossRef]
5. Liang, J.; Feng, J.; Fang, Z.; Lu, Y.; Yin, G.; Mao, X.; Wu, J.; Wang, F. An Energy-Oriented Torque-Vector Control Framework for Distributed Drive Electric Vehicles. *IEEE Trans. Transp. Electrification* **2023**, *9*, 4014–4031. [CrossRef]
6. Liang, J.; Wang, F.; Feng, J.; Zhao, M.; Fang, R.; Pi, D.; Yin, G. A Hierarchical Control of Independently Driven Electric Vehicles Considering Handling Stability and Energy Conservation. *IEEE Trans. Intell. Veh.* **2023**, *9*, 738–751. [CrossRef]
7. Du, J.; Wang, X.; Lv, H. Optimization of magnet shape based on efficiency map of IPMSM for EVs. *IEEE Trans. Appl. Supercond.* **2016**, *26*, 0609807. [CrossRef]
8. Zhang, Z.; Zuo, C.; Hao, W.; Zuo, Y.; Zhao, X.L.; Zhang, M. Three-speed Transmission System for Purely Electric Vehicles. *Int. J. Automot. Technol.* **2013**, *14*, 773–778. [CrossRef]
9. Jung, H.-C.; Kim, D.-J.; Jung, S.-Y.; Lee, D. Optimization Method to Maximize Efficiency Map of a Drive Motor With Electrical Winding Changeover Technique for Hybrid EV. *IEEE Trans. Appl. Supercond.* **2020**, *30*, 5205405. [CrossRef]
10. Zhou, X.; Yang, J.; Migliazza, G.; Guenter, S.; Wang, S.; Gerada, C.; Buticchi, G. Improved Speed Extension for Permanent Magnet Synchronous Generators by Means of Winding Reconfiguration. *Energies* **2023**, *16*, 899. [CrossRef]
11. Hsieh, M.; Hsu, F.; Dorrell, D.G. Winding changeover permanent-magnet generators for renewable energy applications. *IEEE Trans. Magn.* **2012**, *48*, 4168–4171. [CrossRef]
12. Wang, M.; Hsu, N.; Chiang, C.; Wang, S.; Shau, T. A novel changeover technique for variable-winding brushless DC motor drives. In Proceedings of the SICE Annual Conference 2010, Taipei, Taiwan, 18–21 August 2010.
13. Kume, T.; Iwakane, T.; Sawa, T.; Yoshida, T.; Nagai, I. A wide constant power range vector-controlled ac motor drive using winding changeover technique. *IEEE Trans. Ind. Appl.* **1991**, *27*, 934–939. [CrossRef]
14. Kume, T.; Sawa, T.; Sawamura, M.; Zenke, M. Inverter Driving Method for Induction Motors. U.S. Patent 4/916,376, 10 April 1990.
15. Yano, A.; Shimizu, D.; Yano, K.; Momen, K. Electric Motor Drive System and Winding Switching Method. U.S. Patent 14/598,177, 5 January 2015.
16. Kume, T.; Sawa, T. A Static Winding Changeover Technique. Japanese Patent Hei 7-99959, 25 October 1995.
17. Swamy, M.M.; Kume, T.; Maemura, A.; Morimoto, S. Extended High-Speed Operation via Electronic Winding-Change Method for AC Motors. *IEEE Trans. Ind. Appl.* **2006**, *42*, 742–753. [CrossRef]
18. Sadeghi, S.; Guo, L.; Toliyat, H.A.; Parsa, L. Wide Operational Speed Range of Five-Phase Permanent Magnet Machines by Using Different Stator Winding Configurations. *IEEE Trans. Ind. Electron.* **2012**, *59*, 2621–2631. [CrossRef]
19. Itoh, J.-I.; Tanimukai, K. Seamless star-delta winding changeover circuit for AC generators. In Proceedings of the 2015 International Conference on Renewable Energy Research and Applications (ICRERA), Palermo, Italy, 22–25 November 2015.
20. Takatsuka, Y.; Hara, H.; Yamada, K.; Maemura, A.; Kume, T. A wide speed range high efficiency EV drive system using winding changeover technique and SiC devices. In Proceedings of the IPEC Hiroshima 2014 ECCE-ASIA, Hiroshima, Japan, 18–21 May 2014; pp. 1898–1903.
21. Maemura, A.; Morimoto, S.; Yamada, K.; Sawa, T.; Kume, T.J.; Swamy, M.M. A Novel Method for Extending Stroke Length in Moving Magnet Type Linear Motor Drive System by Employing Winding Changeover Technique. In Proceedings of the IEEJ International Power Electronics Conference 2005, Tokyo, Japan, 4–8 April 2005.
22. Kume, T.; Swamy, M.M.; Sawamura, M.; Yamada, K.; Murokita, I. A Quick Transition Electronic Winding Changeover Technique for Extended Speed Ranges. In Proceedings of the IEEE Power Electronics Specialists Conference, Aachen, Germany, 20–25 June 2004.
23. Shin, Y.; Na, J.; Cho, S.; Park, J.; Shin, W.; Lee, J. A Study on the Winding Changeover Circuit to Expand the High Efficient Operating Region of EV Traction Motor. In Proceedings of the 2021 24th International Conference on Electrical Machines and Systems (ICEMS), Gyeongju, Republic of Korea, 31 October–3 November 2021.